Surfaces of a Colloidal Iron Nanoparticle in Its Chemical Environment: A DFT Description

Guntram Fischer, Romuald Poteau, Sebastien Lachaize, I.C. Gerber

Surfaces of Colloidal Iron Nanoparticle in its Chemical Environment: a DFT Description

Guntram Fischer, Romuald Poteau, Sébastien Lachaize, and Iann C. Gerber*

Université de Toulouse; INSA, UPS, CNRS; LPCNO, 135 Avenue de Rangueil, 31077 Toulouse, France

E-mail: igerber@insa-toulouse.fr

Abstract

Describing and understanding surface chemistry at the atomic scale is of primary importance in order to predict and rationalize nanoparticle morphology as well as their physical and chemical properties. Here we present the results of comprehensive density functional theory studies on the adsorption of several small organic species, representing the major species (H_2, Cl_2, HCl, NH_3, NH_4Cl, and CH_3COOH), present in reaction medium during colloidal iron nanoparticle synthesis, on various low-indexed iron surface models, namely (100), (110), (111), (211), and (310). All tested ligands strongly interact with the proposed surfaces. Surface energies are calculated and ligand effects on the morphologies are presented, including temperature effects, based on a thermodynamic approach combined with the Wulff construction scheme. The importance of taking into account vibrational contributions during the calculation of surface energies after adsorption is clearly demonstrated. More importantly, we find that thermodynamic ligand effects can be ruled out as the unique driving force in the formation of recently experimentally observed iron cubic nanoparticles.

*To whom correspondence should be addressed

Introduction

Metallic iron is a promising material in an enormous range of application fields involving nanoparticles (NPs). This includes not only modern technologies such as spintronics or biomedical applications,[1–4] but as well "classical" fields such as catalysis.[5,6] In order to be able to correctly describe and predict the processes and properties of the involved materials in such surface sensitive areas, it is of fundamental importance to understand the interaction of the iron with its environment. One elegant way to yield size-controlled Fe nanoparticles (FeNPs) with specific, in particular cubic, morphologies is to grow them in liquid-phase reactions under mild conditions.[7,8] The reduction of an organometallic precursor in a non-polar solvent (mesitylene) under H_2 pressure, combined with a careful choice of stabilising ligands, ensures controlled surface states free of oxidation. As environment effects are of primary importance for the morphology, the precursor choice plays a crucial role in NP structure,[9,10] assuming that some precursor residues can be coordinated on the surface of the nanocluster. It has also been stated that acid/amine ratio is a central parameter for the morphology of FeNPs.[11,12]

Employing first-principles calculations allows for the calculation of ligand-induced changes of the surface energies, including temperature effects. By building computed phase diagrams,[13] NP shapes can be predicted thanks to Wulff constructions.[14] This has to some extent already been done for the case of iron surfaces and several ligands, in particular for several low-indexed bare facets.[15–18] H adsorption has intensively been studied computationally as well.[19–25] Further studies on the other ligands investigated in the present paper also exist, such as on Cl species[26] and NH_3.[25,27–30] For the latter, a systematic study of the adsorption on a $Fe_5$5 NP model has been also proposed.[31] However, no systematic, consistent, and comprehensive first-principles investigations on the adsorption of HCl, NH_3, NH_4Cl, and CH_3COOH have been proposed, despite their presence during chemical synthesis of FeNPs.[9,32–35] Modeling CH_3COOH and NH_3 adsorption may give insights on the effects of the presence of long aliphatic chain carboxylic acids and amines, usually used as stabilizing

agents.

In this paper we present calculations within the Density Functional Theory (DFT) framework on the adsorption of atomic H, atomic Cl and the four above mentioned molecules. The investigated surfaces, (100), (110), (111), (211), and (310), are modeled by a slab approach in periodic boundary conditions. The results should, thus, be valid for a wide range of sizes of experimental systems, with typical dimensions above a few nanometers.[36]

Our first focus is put on adsorption energies as well as on surface energies including temperature effects through thermodynamic and vibrational contribution, in order to predict FeNP shapes. Secondly, the adsorption strength of H, Cl, and NH_3 species is also rationalized using a recently proposed DFT-based descriptor[37] readily derived from the *d*-band center model of Hammer and Nørskov.[38,39] This generalized ligand-field theory allows to understand the local surface properties of metal surfaces and NPs, in terms of molecular orbital interactions.

This paper is outlined as follows: the next section sketches the main technical and methodological details, more details are given in supporting information when needed. The results, sorted by ligands, are then presented and discussed. Conclusions are finally given.

Theoretical Details

Electronic Structure Calculations

The DFT calculations were done in the generalized gradient approximation in the PBE parametrization[40] within the Vienna ab initio simulation package (VASP).[41,42] The projector augmented wave method[43] was employed and an energy cut-off of 400 eV was chosen.

2×2 surface unit cells with a Fe slab thickness of 9 monolayers (ML) and, in the case of the (310) surface, 11 ML, were used to model the surfaces. For each surface cell the thickness of the vacuum region was larger than 16 Å. The three (five in the case of (310)) central ML were kept at the theoretically determined Fe bulk lattice constant of 2.84 Å, all

other Fe and ligand atoms were allowed to relax using the RMM-DIIS method,[44] with a force convergence criterion of $0.02\,\mathrm{eV\AA^{-1}}$. Atomic charges were estimated employing the Bader charge analysis.[45,46]

In order to find the preferred adsorption sites for each ligand, several high symmetry positions were tested as shown in Figure 1.

Note that the areas of the (2×2) surface cells of the different facets differ, the precise values being listed in Table 1. The coverage value, i.e the number n of ligands per (2×2) surface cell, was used as a varying parameter. In case of atomic adsorption (H and Cl), the coverage of the surfaces in units of ML is determined via $n/4$.

Adsorption and Surface Energies

The surface energy γ_{hkl} is the quantity determining the stability of the surface with the Miller index hkl. For the bare case, indicated by the upper index b, it is defined via

$$\gamma^b_{hkl} = \frac{1}{2A_{hkl}} \left(E_{hkl} - N E_{\mathrm{bulk}}\right) \ , \tag{1}$$

where A_{hkl} is the surface area of the used cell. E_{hkl} is the total energy of the slab cell consisting of N Fe atoms ($N = 36$, or 44 for the (310)) and E_{bulk} represents the total energy of one Fe atom in the bulk phase. The factor $1/2$ is due to the fact that the slab has two surfaces. Both energies are directly obtained from DFT calculations at 0 K.

In case of ligands adsorbed on a surface the surface energy is generally defined via

$$\gamma_{hkl} = \gamma^b_{hkl} + \frac{\Delta_a G_{hkl,n\mathrm{L}}(T,a)}{2A_{hkl}} \ . \tag{2}$$

$\Delta_a G_{hkl,n\mathrm{L}}(T,a)$ is the Gibbs free energy of adsorption of all n_i ligands L_i ($\sum_i n_i \mathrm{L}_i$ shortened to $n\mathrm{L}$) of species i on the surface (hkl). It corresponds to the reaction $(hkl) + \sum n_i \mathrm{L}_i \rightarrow \sum n_i \mathrm{L}^*_i(hkl)$, at temperature T and activity a. At $T = 0\,\mathrm{K}$ when neglecting any thermody-

namic contributions to the Gibbs free energy, $\Delta_a G_{hkl,n\mathrm{L}}(T,a)$ takes the form

$$\Delta_a G_{hkl,n\mathrm{L}}(0,0) = E_{\mathrm{ads}} = E_{n\mathrm{L}^*(hkl)} - E_{(hkl)} - nE_{\mathrm{L}} \ , \tag{3}$$

where E_{ads} is called adsorption energy containing only electronic contributions. The activity is a general term and represents different quantities depending on the experimental conditions and environment. In particular, a assumes the pressure p in case of the perfect gas or molarity c in case of an infinitely diluted solution. Accordingly, a° represents either the standard pressure p° or a standard molarity c°. The ratio a/a° was used as a parameter to study the temperature effects on the surface energies at different environmental conditions. Having determined surface energies γ_{hkl} of a crystal, it is straightforward to perform the Wulff construction which predicts the thermodynamically stable shape of a single crystal NP.[14]

Construction of a *d*-Band Center Based Coordination Map

As shown in a previous paper for Ru NPs,[37] the adsorption strength for a given coordination site μ_k can be assessed by calculating an index, $\bar{\varepsilon}_d(\mu_k)$, with k the coordination number. This index can be nicely depicted as a color map, which provides a first overview of the d-accessibility of a μ_k site. It is calculated as the normalized, energy-weighted integral of the density of states (DOS), projected onto *all* d atomic orbitals (AOs) of the surface atoms which characterize the μ_k coordination site,

$$\bar{\varepsilon}_d(\mu_k) = \frac{\left(\sum_{a\in\mu_k}\sum_m \int_{E_{\min}}^{E_{\max}} \epsilon n_{d_m}(a,\epsilon)d\epsilon\right)}{\left(\sum_{a\in\mu_k}\sum_m \int_{E_{\min}}^{E_{\max}} n_{d_m}(a,\epsilon)d\epsilon\right)} \ , \tag{4}$$

where m runs over the five d AOs and $n_{d_m}(a,\epsilon)$ is the atom-projected density of states on the d_m AO of atom a; μ_k is reminiscent of the symbol which designates bridging ligands in coordination chemistry and the bar sign above ε_d means that it is averaged over all d AOs.

If the summation in Equation (4) is omitted and m kept fixed, the center of this specific d orbital, $\varepsilon_{d_m}(a)$, is calculated. This allows to analyse a possible covalent adsorption process in terms of $\varepsilon_{d\sigma}$, $\varepsilon_{d\pi}$ and $\varepsilon_{d\delta}$ indices. See the supporting information for more details.

Results and Discussion

Bare Surfaces

The bare surface energies γ^b_{hkl}, calculated via Equation (1), are given in Table 1. They are in good agreement with previous theoretical works, with results differing by less than 3% from recent studies.[16,18,47] The (110) facet has the lowest surface tension, followed by the (100). Interestingly the naked quasi-stepped surfaces (211) and (310) are more stable than the low crystallographic indexed (111) surface. The resulting Wulff shape at $T = 0$ K, shown in Figure 2, is almost spherical, as already found in Reference 18.

Table 1: Surface energies γ^b_{hkl} and the corresponding area of the (2×2) surface cell.

hkl	(100)	(110)	(111)	(211)	(310)
γ^b_{hkl} / J/m^2	2.47	2.41	2.65	2.56	2.50
A / Å^2	32.29	22.83	55.92	39.54	51.05

It confirms that the chemical environment plays a crucial role, during organometallic synthesis of FeNPs, since cubic shapes, exhibiting (100) facets, are experimentally observed for NPs $\gtrsim 5$ nm.[32–34,48] The presence of ligands at the surface of the NP should inverse the relative stability of the (100) over the (110) surface. Since the surface ratio is in favor of the (110) surface by a factor of around 0.7, according to Equation (2) ligands able to compensate this imbalance will have to adsorb more strongly to the (100) surface. This may append due to stronger chemical bonding per ligand or due to a higher coverage value, since the (100) facet has a larger area.

The $\bar{\varepsilon}_d(\mu_k)$ index for each slab, reported in Figure 3(a), provides a first prediction of the chemisorbed species adsorption strength on metallic surfaces. The correspondence between

colors and energy scale for the construction of d-band center coordination maps of iron surfaces is shown on top of Figure 3(a). When $\bar{\varepsilon}_d(\mu_k)$ is close to the Fermi level, the site is colored in red, meaning that the adsorption is strong. When the site is in blue, the adsorption strength is weaker. The surface Fe(110) average d-band center value (-1.63 eV) was chosen as the origin of this scale (*i.e.* white), whereas the bottom of the scale is set up to the lowest ε_d, a value found for (100) surface atoms. From figure 3(a) it is clear that simple species are not expected to adsorb more strongly on the (100) plane than on the (110) one, this statement being confirmed by the detailed analysis of the effective d AOs diagram plot in Figure 3(b).

On the basis of these effective d AOs, we can conclude that simple species such as H or Cl atoms should not be able to invert the relative stability of the (100) and (110) surfaces. However, more complex chemical processes, such as dissociative adsorption, could modify this simple picture. For instance a significant surface polarization will modify the local accessibility of the metal d AOs in the neighborhood of the sites involved in this co-adsorption process. Interestingly, tilted adsorption of σ-donor ligands on the (111), (211) and (310) planes may be favored by the d_π or d_δ AOs of the surface atoms. Besides, coordination modes involving the second layer atoms is also possible, due to their energetic accessibility (Figure 3(b), blue levels). The d_π levels are almost degenerate in all cases and close to the Fermi level. In addition, at least one d_δ of the upper layer atoms also lies high in energy. All these electronic properties may enhance the simultaneous adsorption of simple species on both layers.

H Adsorption

The adsorption of H atoms on Fe surfaces has been well documented in the last years with several theoretical works.[19–22,25,49] These have reported adsorption sites and energies at different coverage values, on a limited number of surfaces models with various computational settings. The latter makes comparisons difficult, when here we present a consistent study.

The main results are compiled in Table 2.

Table 2: Adsorption sites of a single H atom on various surfaces, as defined in Figure 1, with the corresponding Fe-H minimal distances, the highest vibrational frequencies, and the adsorption energies at $T = 0\,K$. The optimal coverage values n_0 resulting in the minimum surface energies $\gamma_{hkl}^{n_0}$ upon H adsorption are also given. The same sites hold for $n = 1$ and n_0 in all cases.

hkl	(100)	(110)	(111)	(211)	(310)
Site	H	3f	Tsb (Qf)[a]	Qt	Qt1
$d_{\min}$ / nm	1.73	1.78	1.63	1.77	1.80
$\bar{\nu}_{hkl}$ / cm^{-1}	1182	1065	1488	1102	1055
$E_{ads}^{n=1}$ / eV	-0.40	-0.70	-0.57	-0.55	-0.65
	-0.38, -0.34, -0.35[b]	-0.71, -0.69, -0.73[c]	-0.56, -0.70[d]	-0.70[e]	-0.54[f]
n_0	4	4	8	4	4
$E_{ads}^{n=n_0}/n_0$ / eV	-0.41	-0.62	-0.49	-0.55	-0.65
$\gamma_{hkl}^{n_0}$ / J/m^2	1.66	0.59	1.54	1.67	1.69

[a] See supporting information for details on the adsorption of 8 H.
[b] Taken from References 20, 49, and 50, respectively.
[c] Taken from References 20, 50, and 29, respectively.
[d] Corresponds to half the value calculated for 2 H atoms in Reference 21.
[e] Taken from Reference 25.
[f] Taken from Reference 49.

Adsorption energies of a single H atom, corresponding to a coverage of 0.25 ML, are in good agreement with previous theoretical works,[19–22,49] except for the (211) surface. If it was previously found that a single H atom prefers the short bridge (Sb) site,[25] the quasi three-fold (Qt) site is slightly more stable here. The energy difference between these two sites is around 0.02 eV, as in the cited paper.[25] We also find that adsorption at the Sb2 site is only approximately 0.01 eV higher in energy than at Qt, meaning that the three sites are equivalent with regards to energy precision.

Although H species at the Fe surfaces does not form pure covalent bonds, the adsorption energy values in Table 2 correspond well to the ε_d map given in Figure 3. The relatively large $E_{ads}^{n=1}$ value of the μ_3 site of the (110) surface can be safely attributed to a much better availability of the d_{xz} and d_{yz} (d_π) orbitals of the surface atoms, when the same orbitals are deeper (0.3 eV), for the μ_4-H sites of the (100) surface. This trend also holds for cubic nano cluster model made of 91 Fe atoms, thus limiting the supposed finite-size effects, where

atoms at the center of the (100) facets and slab surface atoms have similar effective d AOs diagrams, see supplementary information. Besides, the small E_{ads} obtained on the (111) surface seems, at first sight to be in contradiction with the energy level of ε_{d_σ}. But in this particular case there is a large charge re-distribution, disturbing the balance between orbital-driven and charge-driven interactions. Indeed, a large charge transfer, between 0.29 and 0.40 e per H atom depending on the surface orientation is obtained. This transfer, in good agreement with recent experimental findings,[35] is more pronounced for low coverage values and large surface unit cells, i.e by minimizing the lateral interactions between ligands. In the specific case of the (111) surface, the negatively charged H are closer to the second ML of Fe. As the latter is also negatively charged, see Figure 2 in the supporting information, the corresponding adsorption energy gets smaller. This shows that electrostatic effects can modulate expected E_{ads} from a simple d-band center analysis.

From the comparison between values of $\gamma_{hkl}^{n_0}$ in Table 2 at T= 0 K, the fully H-covered (110) surface represents by far the most stable configuration. This is caused by the large adsorption energy per ligands in conjunction with the smallest area of the surface. Thus, starting with spherical seeds of NPs, at very low temperature and under H_2 pressure, (110) surfaces should be largely promoted and dodecahedral NPs covered by 1ML of hydrides as in Figure 4(c), should be yielded.

Including thermodynamic effects on the morphology requires the determination of the adsorbed species vibrations. The highest of the three vibrational excitation frequencies $\bar{\nu}_{hkl}$ of one H adsorbate at each surface are given in Table 2. They correspond to the mode with a large component along the surface normal, but are not necessarily exactly perpendicular to the surface. Their magnitude is reciprocally related to the distance to the nearest Fe atom. The (110) value, $\bar{\nu} = 1065\,\mathrm{cm}^{-1}$, is in excellent agreement with the experimental value of $1060\,\mathrm{cm}^{-1}$.[51] Higher surface coverage generally results in a slight increase of the given $\bar{\nu}_{hkl}$, due to the increased Coulomb repulsion between the H atoms hindering their vibrational movement. The resulting surface energies upon H adsorption including thermodynamics

and vibrational effects, as written in Equation (2), are given in Figure 4. The effects on the surface energies of the vibrational contributions, are clearly demonstrated in Figure 4(b). Without the vibrational terms, the energy values are lower. The temperatures below which adsorption occurs can, thus, be shifted by more than 100 K, as in the case of the (211) and (310) surfaces, due to large differences in the H-frequencies. This agrees well with previous results obtained in the case of H adsorption on Ru (0001) surface.[52]

The activity a of H_2 and the temperature T do have a significant impact on the adsorption behavior, and thus on the predicted morphologies. On one side, for low activities and at high temperature, the adsorption becomes unfavorable, and spherical NPs, made of naked surfaces, are yielded at $450\,K$ for a low activity 10^{-7}, see Figure 4(d). On the other side fully H-covered Fe surfaces are preferred when the temperature is not too high. This seems to be in contradiction with recent experiments on pure Fe(0) NPs, which yield H coverage values between 0.4 and 0.6 ML has been found.[35] But here, stabilizing ligands present in the reaction medium, are not taken into account, and certainly compete with H species to occupy surface sites. When hydrides only are adsorbed, as shown in Figures 4(c), (e), and (f), (110) facets are dominant with a little of (310) surfaces. The effect of temperature is also clear, when $a/a^\circ = 1$, at $T = 150$ K the Fe NP is a rhombic dodecahedron of (110) facets, when the temperature is increased more (100) facets appear. As a consequence the presence of hydrogen alone in the reaction medium is not responsible for the cubic shape of FeNPs.

Cl Adsorption

Table 3 summarizes the main results of the Cl radicals adsorption on Fe surfaces. Although it is unrealistic to consider radicals in the context of colloidal NPs synthesis, Cl^- species are more likely to be present instead, such reference data still remain potentially useful in some other experimental contexts.[53,54]

Chlorine adsorption is energetically favorable on all surfaces, with absolute values of

Table 3: Preferred adsorption sites (see Figure 1) for a Cl radical at the bare surface and the corresponding E_{ads}. The normal vibrational mode frequency ($\bar{\nu}_{hkl}$) upon a single adsorption, the minimum energy coverage values n_0, the corresponding adsorption energies per Cl ligand, and the resulting surface energies are given.

hkl	(100)	(110)	(111)	(211)	(310)
Site	H(B)	Lb	T2	Sb	Qt1
$E_{\mathrm{ads}}^{n=1}$ / eV	-1.46	-1.67	-1.62	-1.69	-1.74
$\bar{\nu}_{hkl}$ / cm^{-1}	158/225	226	211	255	229
n_0	2	2	4	2	4
$E_{\mathrm{ads}}^{n=n_0}/n_0$ / eV	-1.50	-1.06	-1.62	-1.69	-1.38
$\gamma_{hkl}^{n_0}$ / J/m^2	0.98	0.92	0.84	1.18	0.78

E_{ads} considerably larger than in the case of H species. When a single radical is present, the smallest energy gain is on the (100) surface, as for a single H atom, as predicted by the $\bar{\varepsilon}_d(\mu_k)$ index value. Cl radicals prefer to be in μ-positions with d(Fe-Cl) being between 2.30 and 2.35 Å. When Cl atoms interact with a (110) facet, the most stable sites are the long bridge (Lb) ones, contrarily to a previous theoretical result[29] that states the three-fold hollow (3f) site is lower in energy. A possible reason may be too low number of Fe ML (5) used in the cited work, that restricts the relaxation process.

It is only for the (100) case that a change of the adsorption site from H to B occurs when a second ligand is added to the surface. This coordination mode change is a clear evidence of ligands lateral interaction, at a coverage value of $n = 2$. The hollow site H was previously proposed[26] as the most stable site in case of single ligand adsorption. Another consequence of the strong interaction between adsorbed Cl atoms, is that the complete coverage of the surfaces, $n = 4$, is only possible for the two largest surface cells, namely (111) and (310). This result is in good agreement with observations made on the (100) surface,[26,55] where a coverage value of 1ML could not be achieved. Indeed the adsorption of 3 Cl ligands on the 2x2-(100) slab gives a surface energy, $\gamma_{100}^{n=3} = 1.06$ J/m^2, slightly higher than with 2 ligands.

As for hydrogen atom, an electron transfer occurs from the metallic surface to the Cl radical. The negative charge on the ligands lies between 0.50 e and 0.63 e, the minimum being for 2 Cl on the (110) surface and the maximum being for 1 Cl on the (100) slab. The

ionic character is generally more pronounced at low coverage values for larger surface cells, as for H adsorption. This explains the low coverage values yielded on the smallest surfaces, since an extra Cl atom must fight against steric and electrostatic effects simultaneously. As a consequence, the (111) and (310) surfaces have the smallest surface energies, thus these surfaces will be more present in the corresponding Wulff construction.

The highest vibrational frequency of each Cl at the respective surface is listed as well in Table 3. In column (100) the two values correspond to the adsorption of 1 Cl at the H site and 1 Cl at the B site, which is the only occupied site if 2 Cl are trapped on the surface. The reason for the difference between $\bar{\nu}_{100}$ of the H site and all the others sites is related to the Fe-Cl bond-length. As usual, a smaller bond-length means a harder vibrational mode. From these values, the Fe-Cl bonds are very soft compared to H-Fe ones.

HCl Adsorption

Hydrochloric acid solution is often used in the context of colloidal FeNPs synthesis, thus making theoretical investigations of the interaction of HCl molecules with Fe surfaces of first importance. Interestingly HCl spontaneously dissociates, with an adsorption energy of around 2 eV on the different surfaces. The energetic and geometric aspects of the adsorption process are the corresponding main results are summarized in Table 4.

Table 4: Preferred adsorption sites (see Figure 1) for one dissociated HCl molecule written X-Y with X, Y being the site of H and Cl respectively, with the corresponding adsorption energy are given. The highest vibrational frequencies of the a dissociated HCl are also presented followed by the minimum energy coverage values n_0, the corresponding adsorption energies per HCl molecule, and the resulting surface energies.

hkl	(100)	(110)	(111)	(211)	(310)
Site ($n = 1$)	H-B	3f-Lb	Tsb-T2	Qt-Sb	Qt1-Qt1
$E_{\mathrm{ads}}^{n=1}$ / eV	-1.92	-2.18	-2.18	-2.25	-2.38
$\bar{\nu}_{hkl}^{\mathrm{H}}$ / cm^{-1}	1218	1162	1491	1112	1056
$\bar{\nu}_{hkl}^{\mathrm{Cl}}$ / cm^{-1}	229	230	213	261	224
n_0	2	2	3	2	3
$E_{\mathrm{ads}}^{n=n_0}/n_0$ / eV	-1.77	-1.19	-1.80	-2.18	-1.75
$\gamma_{hkl}^{n_0}$ / $\mathrm{J/m}^2$	0.72	0.74	1.11	0.80	0.85

For $n = 1$, *i.e.* for a single HCl molecule, the adsorption sites of H and Cl are the same as the isolated cases with two atomic species adsorbed. In these configurations, the site occupation tend to maximize the distance between the H and Cl atoms. The adsorption energy, $E_{\text{ads}}^{n=1}$, corresponds roughly to the sum of the values of the isolated ligands. An exception to this is the (110) surface, due to its modest surface area that involves a larger Coulomb interaction between negatively charged H and Cl. The frequencies associated to a dissociated HCl molecule, given in Table 4, agree well with those of the single ligands except for the H at (100) and (110) cases, again due to strong lateral interaction.

Increasing the ligand coverage values leads to changes in the coordination modes. The underlying mechanism is again the maximization of the distance between the ligands. This phenomenon is more pronounced on the (100) and (110) surfaces, where H and Cl occupy the same symmetry sites already for $n = 2$. For the (211) case, the H atom moves from the Qt to the Sb2 site. For the surfaces with the largest areas, (111) and (310), with $n = 2$ the adsorption sites remain identical. When $n = 3$, larger rearrangements are observed and presented in the supplementary information.

According to the charge analysis, the adsorbed H ion charge ranges from $0.28\,e$ to $0.38\,e$, when for Cl it becomes $0.52\,e$ to $0.60\,e$. These values are also very close to the isolated case, meaning that co-adsorption has a little effect on the charge transfer between the Fe surface and the adsorbates. This anionic ligand's character reinforces the weakening of the adsorption energies when increasing the coverage values. It is symptomatic in the (110) case, with a reduction of around 50% due to Coulomb repulsion between hydrides and chlorides. Looking at $\gamma_{hkl}^{n=n_0}$ it is found that the (100) and (110) values are the lowest, in the presence of HCl. Despite the strong adsorption energies on the (111) and (310) surfaces and the corresponding larger n_0, they still remain less favorable than the (100) and (110).

The γ_{hkl}, including thermodynamic and vibrational contributions, are shown in Figure 5 for 2 different values of the HCl molarity in the solution. Evidently, adsorption process is strong on all surfaces and takes place at the whole investigated range of temperature and ac-

tivity. The corresponding Wulff structures are sketched in Figures 5(c) to (f). The dominant facets are made of (211), (110), and the (100) surfaces. The latter becomes strongly preferred at favorable conditions of adsorption, *i.e.* high a/a° ratio and low T as in Figure 5(e). When taking into account the thermodynamic and vibrational contributions there is a change of n_0 value for the (110) surface in the investigated range of T and a/a°. Figures 5(a) and (b) clearly show that γ_{110} is lower during the whole T range if $n = 1$ instead of 2. It is, then, reasonable to assume that the remaining surface sites may become occupied by H ligands, as they strongly adsorb on (110) facets. Indeed the most stable configuration is obtained for 3 H and one Cl adsorbed on the (110) surface model, with a surface energy of 0.45 J/m^2.

However, as demonstrated in Figures 5(a) and (b), taking into account as well the thermodynamic and vibrational contributions shows that extra H adsorption are possible only at low temperature and small activity. The difference between the two configurations affects slightly the resulting NP shapes, see Figures 5(c) and (e). Except for the (110) case, all surfaces will be fully covered by hydrides and chlorides. This could be an explanation for the reported value of H coverage around 0.4 and 0.6 ML.[35]

NH_3

Ammonia is a stable molecule with reported dissociation barriers of 0.9 eV at the (100)[27] and of 0.7 eV at the (110)[30] surface. We do, therefore, not observe any N-H activation. Table 5 summarizes results on the adsorption process.

NH_3 molecule adsorbs always on top of surface Fe atom, for all tested surfaces, as in previous studies.[28,29,56] The adsorption always occurs via the N atom with no tilting angle. The corresponding E_{ads} are close to those of H-coverage case. This rather low magnitude, compared to Cl or HCl, is presumably due to the already saturated bonds of the NH_3 molecule. Our computed values can vary from those reported in the literature because of the difference in computational settings.

Charge analysis shows that only small electron transfer occurs between the Fe surface

Table 5: Preferred adsorption sites (see Figure 1) for NH_3 molecules for $n \geq 1$ and the adsorption energies for one adsorbed molecule calculated in this work and, as well, obtained in previous works. Underneath follow minimum energy coverage values n_0 with the corresponding adsorption energies per NH_3 molecule and the resulting surface energies.

hkl	(100)	(110)	(111)	(211)	(310)
Site	T	T	T1	T	T1
$E_{\mathrm{ads}}^{n=1}$ / eV	-0.53	-0.51	-0.85	-0.74	-0.74
$E_{\mathrm{ads}}^{n=1}$ / eV	-0.92[a]	-0.47, -0.73, -0.83[b]	-0.94, -0.70[c]	-0.79[d]	–
n_0	2	1	4	2	4
$E_{\mathrm{ads}}^{n=n_0}/n_0$ / eV	-0.35	-0.51	-0.50	-0.59	-0.44
$\gamma_{hkl}^{n_0}$ / J/m^2	2.13	2.05	2.09	2.08	1.94

[a]Taken from Reference 27
[b]Taken from References 28, 29, and 30 respectively. Reference 30 contains zero-point energies.
[c]Taken from References 28 and 56, respectively.
[d]Taken from Reference 25

and the NH_3 ligands, This means as well that the N-Fe bonds are strongly covalent and the trend of adsorption energies at the different surfaces should be well explained by the $\bar{\varepsilon}_d$ in Figure 3. The lowest values for $\bar{\varepsilon}_d$ and E_{ads} are found for the (100) facet. However, at (110) E_{ads} is surprisingly low, possibly due to the different amounts of charge transfer between the surfaces and the ligand. At the (110) surface the NH_3 adsorbate is neutral. This means that the strength of the adsorption is solely determined by the covalent bond and, thus, by the d-band center. In all other cases the ligand molecule is slightly positively charged, ranging from 0.02 for the (100) to 0.08 e for the (111) case. This small, yet present charge transfer may lead to electronic rearrangements which contribute to the adsorption energy via additional Coulomb interactions between the ligand and the surface or, as well, between the different Fe layers and atoms. In this context it should be noted that this sensitivity of E_{ads} towards fluctuations of the charge can possibly explain the previously obtained scattered values cited in Table 5. Figure 1 in the S.I., illustrates the charge distribution among the different surfaces in case of NH_3 adsorption.

Owing to steric effects, the number of NH_3 molecules that can be adsorbed is small for the unit cells with small surface areas. For instance, adding a second NH_3 molecule on the small (110) surface already results in a surface energy higher than the bare one. Similarly, if

a second ligand is adsorbed on the (100) model, a significant reduction of E_{ads} is obtained. This is less true for the (211) surface, as the dimension in direction perpendicular to the top Fe rows allow for a larger distance between two NH_3. The facet with the lowest surface energy is, then, the (310), since four NH_3 molecules can be adsorbed while maintaining reasonable distances between them. Despite the adsorption energy values, NH_3 will not adsorb in a significant amount on FeNP surfaces. This is caused by thermodynamic contributions (no vibrational yet) which drastically increase the surface energies. For instance, assuming $a/a^\circ = 1$ and $T = 300\,\text{K}$ yields γ_{hkl} of 2.47, 2.40, 2.52, 2.47, and $2.43\,\text{J/m}^2$ for the (100), (110), (111), (211), and (310) surface, respectively. It should be even more pronounced if the vibrational contributions are included.

Regarding the dissociation of NH_3 into its components, it is expected that the adsorbed N recombines with H species from the surrounding environment to reform NH_3 and then desorb.[57] This holds since test calculations on a single N adsorption provide only weak adsorption energies ($|E_{\text{ads}}| < 0.5\,\text{eV}$) on all surfaces, if NH_3 is chosen as nitrogen source. Therefore, it can be concluded that NH_3 molecules will not affect the shape of FeNP in a significant manner.

NH_4Cl

Experimentally, ammonium chloride has been found to directly influence the size of FeNP.[33] Its dissociation into NH_3, H, and Cl above the five considered surfaces and their subsequent adsorption is energetically more favorable than the complex's adsorption. For instance, on the (100) surface the simultaneous adsorption of H, Cl, and NH_3 is about 2 eV lower than that of the whole NH_4Cl. Table 6 summarizes the obtained results.

Table 6: Preferred adsorption sites (see Figure 1) of the dissociated parts of a NH_4Cl molecule (NH_3, H, Cl), together with the adsorption energies.

hkl	(100)	(110)	(111)	(211)	(310)
Site	T-*H*-B	T-3f-3f	T1-Tsb-Tsb	T-Qt-Sb	T1-Qt1-Sb1
$E_{\text{ads}}^{n=1}$ / eV	-2.30	-1.79	-2.62	-2.75	-2.73

The adsorption sites of the three dissociated components are very similar to that of the isolated NH_3 – always on top – and the HCl molecule. In the (100) and (211) cases they are formally identical, while on the other three surfaces, the Cl ligand has been pushed to other neighboring sites, due to the spatial extent of the NH_3 ligand. As a consequence, the adsorption energies values are smaller than the sum of $E_{\mathrm{ads}}^{\mathrm{NH_3}}$ and $E_{\mathrm{ads}}^{\mathrm{HCl}}$. At the (110) surface, $E_{\mathrm{ads}}^{\mathrm{NH_4Cl}}$ is smaller than $E_{\mathrm{ads}}^{\mathrm{HCl}}$. It means that from a dissociated NH_4Cl molecule only the HCl part would actually adsorb. On this basis, for the other 4 surfaces it can be concluded that, in the presence of NH_4Cl in the synthesis medium, only HCl would eventually adsorb, since it always leads to lower surface energies.

CH_3COOH

Having investigated HCl, which corresponds to a strong acid, we have also studied the adsorption of acetic acid, a typical weak acid. Generally, the adsorption of CH_3COOH on the five surfaces is energetically favorable. As in the case of HCl, the configuration with dissociated H and CH_3COO parts are more stable. The respective adsorption geometries are depicted in Figure 6.[58]

The CH_3COO^- adsorbs with its two O atoms on the surface, where the two O are bridging two neighbors surface Fe atoms. The adsorption site of the hydride, since negative charge is observed, corresponds to that of the HCl case as given in Table 4 for $n = 1$. Both oxygen atoms also carry a strong negative charge between -1.1 and -1.2 e. The exact position of each O depends of the specific surface geometry, see Figure 6. Again, these positions are mainly influenced by the Coulomb repulsion between the H and the nearest O. As an example, on the (110) surface (Figure 6(b)), the O atom closer to the H is pushed towards the Sb site. The respective adsorption energies are listed in Table 7. They strongly depend on the distance between the adsorbed acetate and hydride ion. E_{ads} is the largest for the (310) surface, since $d(\mathrm{O}-\mathrm{H})$ is also the largest. Contrarily, it is the weakest for the smallest distance, *i.e* in the (110) case.

Table 7: The adsorption energy E_{ads} of one CH_3COOH molecule, the shortest distance $d(\mathrm{O}-\mathrm{H})$ between an oxygen and the adsorbed hydrogen, the minimum surface energy coverage values n_0 (in number of molecules per calculation cell), with the corresponding adsorption energies per molecule and the resulting surface energies are presented.

hkl	(100)	(110)	(111)	(211)	(310)
E_{ads} [eV]	-1.73	-1.36	-1.97	-1.87	-2.14
$d(\mathrm{O}-\mathrm{H})$ [Å]	2.98	2.61	3.29	3.30	3.55
n_0	2	1	2	2	2
$E_{\mathrm{ads}}^{n=n_0}/n_0$ / eV	-1.50	-1.36	-1.83	-1.67	-1.89
$\gamma_{hkl}^{n_0}$ / J/m^2	0.99	1.46	1.61	1.20	1.31

Adding a second ligand, consisting also of an acetate and a hydride, does not significantly affect the respective adsorption positions. Due to the large volume of the acetate the coverage values leading to the lowest surface energies, n_0, equals 2 with the exception of the (110) case where only one dissociated ligand can be favorably adsorbed. From the minimum surface energies at $T = 0\,\mathrm{K}$ in Table 7, the (100) facet is, by far, the most energetically favorable one. The $\gamma_{310}^{n_0}$ value is already 20 % larger. This huge difference can be attributed to the relatively small surface area being able to adsorb two ligand molecules, leading to a relatively large concentration of energy-reducing ligands at the surface.

This large preference for the (100) surface is weakened if thermodynamic and, in particular, vibration energies are taken into account. Indeed these increases of $\gamma_{(hkl)}$ values for all facets will lead to a drastic reduction of the relative differences between them. As a consequence the (100) facet is definitively less preferred. This is demonstrated in the corresponding Wulff constructions of Figures 7(a) to (d). At low temperatures, there is a strong presence of the (100), (211), and (310) facets, with an increase in the (100) ratio with growing activity. At a higher temperature, adsorption is only weak or not occurring as illustrated in Figure 7(b). In this case, the shape is very similar to the one of a bare Fe NP. Increasing a/a° ratio favors (310) instead of (100) facets, due to different vibrational spectrum of the ligands at the surface. Note as well that the presence of (111) facets is found only in the case of higher temperatures. The presence of CH_3COOH ligands can, therefore, not explain the experimentally observed cubic structures of Fe NP. At experimental condi-

tions thermodynamics rather predict spherical shapes. It can be assumed that this result can be extrapolated to other weak and, as well, long-chained acids that are used in FeNP synthesis, such as palmitic acid.[7]

Summary and Conclusions

We have presented the results of comprehensive DFT calculations about the adsorption of H, Cl, HCl, NH_3, NH_4Cl, and CH_3COOH ligands on five low-indexed Fe surfaces, being (100), (110), (111), (211), and (310). When not considering thermodynamic and vibrational contributions we find that, in general, adsorption is energetically favorable and the surface energies can be significantly lowered compared to the respective bare cases. For simple species (H, Cl and NH_3), adsorption energies at the low concentration limit can be understood in terms of orbital-driven arguments while considering as well the charge distribution between the Fe layers and, likewise, the ligands.

We have demonstrated, as well, that including thermodynamic and vibrational contributions to the calculation of the free Gibbs energy of adsorption leads to an increase of the surface energies, which may in turn, depending on the specific ligands, result in preference for naked surfaces. In particular, it appears essential to include the vibrational part.

Finally, we have shown, owing to the Wulff constructions resulting from thermdoynamics considerations, that of all the considered possible ligands will affect the morphology of the NPs in a signicant manner. As an example, the adsorption of H, a species expected to be abundant on the surface, is predicted to result in perfect dodecahedrons. But, adsorbed species are not the reason for the occurrence of cubic FeNPs in experiments. This is summarized in the phase diagram in Figure 8, showing the trend towards cubic or dodecahedral shapes of ligand-covered FeNPs in dependence on γ_{100} and γ_{110}. All investigated compounds show, if at all, only weak tendencies towards cubic morphology, since they are unable to raise γ_{100} with respect to γ_{110}.

All investigated compounds show, if at all, only weak tendencies towards cubic morphology. Moreover, the adsorption of H, a species expected to be abundant on the surface, is predicted to result in perfect dodecahedrons. The transition towards cubic NPs would involve to raise γ_{110} as well as to lower γ_{100}.

In addition to the calculation of effective surface energies, the coordination d-band center also demonstrates that no electronic effect can invert the relative thermodynamic stability of the (100) and (110) iron surfaces upon adsorption of simple species. Dissociative adsorption processes or co-adsorbed species could possibly change these conclusions, but it is to be expected that cubic NPs do not represent the thermodynamic equilibrium configurations but rather that their growth is governed by kinetics, such as the dissociation of the precursor above the bare or covered surfaces. This will be the topic of a forthcoming paper.

Acknowledgement

The authors thank the ANR for the financial support through the funded project INANOPROCE (Projet ANR-11-JS10-0007). They also thank the CALcul en MIdi-Pyrénés (CALMIP, grant 2011/2013-P0843) for generous allocation of computer time. Part of this work was also performed using HPC resources from GENCI-CINES (Grant 2011/2013-096940), GENCI-CCRT (Grant 2011/2013-096940) and GENCI-IDRIS (Grant 2012/2013-096940).

Supporting Information Available

A detailed description of the computational and technical details is given in the supporting information. Additional results, that help to understand the main aspects of the article, are given as well. This material is available free of charge via the Internet at `http://pubs.acs.org/`.

References

(1) Huber, D. L. Synthesis, Properties, and Applications of Iron Nanoparticles. *Small* **2005**, *1*, 482–501.

(2) Bader, S. D. *Colloquium* : Opportunities in nanomagnetism. *Rev. Mod. Phys.* **2006**, *78*, 1–15.

(3) Qiang, Y.; Antony, J.; Marino, M.; Pendyala, S. Synthesis of core-shell nanoclusters with high magnetic moment for biomedical applications. *Magnetics, IEEE Transactions on* **2004**, *40*, 3538–3540.

(4) Pankhurst, Q. A.; Connolly, J.; Jones, S. K.; Dobson, J. Applications of magnetic nanoparticles in biomedicine. *Journal of Physics D: Applied Physics* **2003**, *36*, R167.

(5) Dry, M. E. The Fischer-Tropsch process: 1950-2000. *Catalysis Today* **2002**, *71*, 227 – 241, Fischer-Tropsch synthesis on the eve of the XXI Century.

(6) Moisala, A.; Nasibulin, A. G.; Kauppinen, E. I. The role of metal nanoparticles in the catalytic production of single-walled carbon nanotubes a review. *Journal of Physics: Condensed Matter* **2003**, *15*, S3011.

(7) Lacroix, L.-M.; Lachaize, S.; Falqui, A.; Respaud, M.; Chaudret, B. Iron Nanoparticle Growth in Organic Superstructures. *Journal of the American Chemical Society* **2009**, *131*, 549–557, PMID: 19140793.

(8) Lu, A.-H.; Salabas, E.; Schüth, F. Magnetic Nanoparticles: Synthesis, Protection, Functionalization, and Application. *Angewandte Chemie International Edition* **2007**, *46*, 1222–1244.

(9) Lacroix, L.-M.; Lachaize, S.; Falqui, A.; Blon, T.; Carrey, J.; Respaud, M.; Dumestre, F.; Amiens, C.; Margeat, O.; Chaudret, B.; Lecante, P.; Snoeck, E. Ul-

trasmall iron nanoparticles: Effect of size reduction on anisotropy and magnetization. *Journal of Applied Physics* **2008**, *103*, 07D521.

(10) Ling, T.; Zhu, J.; Yu, H.; Xie, L. Size Effect on Crystal Morphology of Faceted Face-Centered Cubic Fe Nanoparticles. *The Journal of Physical Chemistry C* **2009**, *113*, 9450–9453.

(11) Farrell, D.; Cheng, Y.; McCallum, R. W.; Sachan, M.; Majetich, S. A. Magnetic Interactions of Iron Nanoparticles in Arrays and Dilute Dispersions. *The Journal of Physical Chemistry B* **2005**, *109*, 13409–13419.

(12) Yang, H.; Ito, F.; Hasegawa, D.; Ogawa, T.; Takahashi, M. Facile large-scale synthesis of monodisperse Fe nanoparticles by modest-temperature decomposition of iron carbonyl. *Journal of Applied Physics* **2007**, *101*, 09J112.

(13) Reuter, K.; Scheffler, M. Composition, structure, and stability of $RuO_2(110)$ as a function of oxygen pressure. *Phys. Rev. B* **2001**, *65*, 035406.

(14) Wulff, G. Zur Frage der Geschwindigkeit des Wachstums und der Auflösung der Krystallflächen. *Zeitschrift für Krystallographie und Mineralogie* **1901**, *34*, 448.

(15) Vitos, L.; Ruban, A.; Skriver, H.; Kollár, J. The surface energy of metals. *Surface Science* **1998**, *411*, 186 – 202.

(16) Błoński, P.; Kiejna, A. Calculation of surface properties of bcc iron. *Vacuum* **2004**, *74*, 179 – 183, Proceedings of the International Workshop on Surface Physics: Metals on Solid Surfaces.

(17) Šipr, O.; Košuth, M.; Ebert, H. Magnetic structure of free iron clusters compared to iron crystal surfaces. *Phys. Rev. B* **2004**, *70*, 174423.

(18) Błoński, P.; Kiejna, A. Structural, electronic, and magnetic properties of bcc iron surfaces. *Surface Science* **2007**, *601*, 123 – 133.

(19) Jiang, D.; Carter, E. A. Adsorption and diffusion energetics of hydrogen atoms on Fe(110) from first principles. *Surface Science* **2003**, *547*, 85 – 98.

(20) Jiang, D. E.; Carter, E. A. Diffusion of interstitial hydrogen into and through bcc Fe from first principles. *Phys. Rev. B* **2004**, *70*, 064102.

(21) Huo, C.-F.; Li, Y.-W.; Wang, J.; Jiao, H. Surface Structure and Energetics of Hydrogen Adsorption on the Fe(111) Surface. *The Journal of Physical Chemistry B* **2005**, *109*, 14160–14167.

(22) Ferrin, P.; Kandoi, S.; Nilekar, A. U.; Mavrikakis, M. Hydrogen adsorption, absorption and diffusion on and in transition metal surfaces: A {DFT} study. *Surface Science* **2012**, *606*, 679 – 689.

(23) Zou, C.; Duin, A.; Sorescu, D. C. Theoretical Investigation of Hydrogen Adsorption and Dissociation on Iron and Iron Carbide Surfaces Using the ReaxFF Reactive Force Field Method. *Topics in Catalysis* **2012**, *55*, 391–401.

(24) Sorescu, D. C. First principles calculations of the adsorption and diffusion of hydrogen on Fe(100) surface and in the bulk. *Catalysis Today* **2005**, *105*, 44 – 65.

(25) McKay, H. L.; Jenkins, S. J.; Wales, D. J. Theory of $NH_x \pm H$ Reactions on Fe{211}. *The Journal of Physical Chemistry C* **2009**, *113*, 15274–15287.

(26) Pick, Š. Comparison of chlorine and oxygen adsorption on the ferromagnetic Fe(001) surface: Density-functional theory study. *Surface Science* **2008**, *602*, 3733 – 3736.

(27) Yeo, S. C.; Han, S. S.; Lee, H. M. Mechanistic Investigation of the Catalytic Decomposition of Ammonia (NH_3) on an Fe(100) Surface: A DFT Study. *The Journal of Physical Chemistry C* **2014**, *118*, 5309–5316.

(28) Satoh, S.; Fujimoto, H.; Kobayashi, H. Theoretical Study of NH_3 Adsorption on Fe(110) and Fe(111) Surfaces. *The Journal of Physical Chemistry B* **2006**, *110*, 4846–4852.

(29) Taylor, C. D. Predictions of Surface Electrochemistry of Saturated and Alkaline NH_4Cl Solutions Interacting with Fe(110) from Ab Initio Calculations. *Corrosion* **2012**, *68*, 591 – 599.

(30) Duan, X.; Ji, J.; Qian, G.; Fan, C.; Zhu, Y.; Zhou, X.; Chen, D.; Yuan, W. Ammonia decomposition on Fe(110), Co(111) and Ni(111) surfaces: A density functional theory study. *Journal of Molecular Catalysis A: Chemical* **2012**, *357*, 81 – 86.

(31) Lanzani, G.; Laasonen, K. NH_3 Adsorption and Dissociation on a Nanosized Iron Cluster. *Int. J. Hydrogen Energ.* **2010**, *35*, 6571 – 6577.

(32) Dumestre, F.; Chaudret, B.; Amiens, C.; Renaud, P.; Fejes, P. Superlattices of Iron Nanocubes Synthesized from Fe[N(SiMe3)2]2. *Science* **2004**, *303*, 821–823.

(33) Meffre, A.; Lachaize, S.; Gatel, C.; Respaud, M.; Chaudret, B. Use of long chain amine as a reducing agent for the synthesis of high quality monodisperse iron(0) nanoparticles. *J. Mater. Chem.* **2011**, *21*, 13464–13469.

(34) Trunova, A. V.; Meckenstock, R.; Barsukov, I.; Hassel, C.; Margeat, O.; Spasova, M.; Lindner, J.; Farle, M. Magnetic characterization of iron nanocubes. *Journal of Applied Physics* **2008**, *104*, –.

(35) Kelsen, V.; Wendt, B.; Werkmeister, S.; Junge, K.; Beller, M.; Chaudret, B. The use of ultrasmall iron(0) nanoparticles as catalysts for the selective hydrogenation of unsaturated C-C bonds. *Chem. Commun.* **2013**, *49*, 3416–3418.

(36) Sun, C. Q. Size dependence of nanostructures: Impact of bond order deficiency. *Progress in Solid State Chemistry* **2007**, *35*, 1 – 159.

(37) del Rosal, I.; Mercy, M.; Gerber, I. C.; Poteau, R. Ligand-Field Theory-Based Analysis of the Adsorption Properties of Ruthenium Nanoparticles. *ACS Nano* **2013**, *7*, 9823–9835.

(38) Hammer, B.; Nørskov, J. Electronic factors determining the reactivity of metal surfaces. *Surface Science* **1995**, *343*, 211 – 220.

(39) Hammer, B.; Nørskov, J. In *Impact of Surface Science on Catalysis*; Bruce C. Gates, H. K., Ed.; Advances in Catalysis; Academic Press, 2000; Vol. 45; pp 71 – 129.

(40) Perdew, J. P.; Burke, K.; Ernzerhof, M. Generalized Gradient Approximation Made Simple. *Phys. Rev. Lett.* **1996**, *77*, 3865–3868.

(41) Kresse, G.; Hafner, J. Ab initio molecular dynamics for liquid metals. *Phys. Rev. B* **1993**, *47*, 558.

(42) Kresse, G.; Furthmüller, J. Efficiency of ab-initio total energy calculations for metals and semiconductors using a plane-wave basis set. *Comput. Mat. Sci.* **1996**, *6*, 15.

(43) Blöchl, P. E. Projector augmented-wave method. *Phys. Rev. B* **1994**, *50*, 17953–17979.

(44) Wood, D. M.; Zunger, A. A new method for diagonalising large matrices. *Journal of Physics A: Mathematical and General* **1985**, *18*, 1343.

(45) Bader, R. F. W. *Atoms in Molecules: A Quantum Theory*; Oxford University Press, 1990.

(46) Tang, W.; Sanville, E.; Henkelman, G. A grid-based Bader analysis algorithm without lattice bias. *Journal of Physics: Condensed Matter* **2009**, *21*, 084204.

(47) Spencer, M. J.; Hung, A.; Snook, I. K.; Yarovsky, I. Density functional theory study of the relaxation and energy of iron surfaces. *Surface Science* **2002**, *513*, 389 – 398.

(48) Margeat, O.; Dumestre, F.; Amiens, C.; Chaudret, B.; Lecante, P.; Respaud, M. Synthesis of iron nanoparticles: Size effects, shape control and organisation. *Progress in Solid State Chemistry* **2005**, *33*, 71 – 79, Advanced Functional Nanomaterials - from NanoscaleObjects to Nanostructered Inorganic and Hybrid Materials.

(49) Carone Fabiani, F.; Fratesi, G.; Brivio, G. P. Adsorption of H_2S, HS, S, and H on a stepped Fe(310) surface. *The European Physical Journal B* **2010**, *78*, 455–460.

(50) Eder, M.; Terakurai, K.; Hafner, J. Initial stages of oxidation of (100) and (110) surfaces of iron caused by water. *Phys. Rev. B* **2001**, *64*, 115426.

(51) Bar, A.; Erley, W. The chemisorption of hydrogen on a (110) iron crystal studied by vibrational spectroscopy (EELS). *Surface Science Letters* **1981**, *112*, L759 – L764.

(52) del Rosal, I.; Truflandier, L.; Poteau, R.; Gerber, I. C. A Density Functional Theory Study of Spectroscopic and Thermodynamic Properties of Surfacic Hydrides on Ru (0001) Model Surface: The Influence of the Coordination Modes and the Coverage. *The Journal of Physical Chemistry C* **2011**, *115*, 2169–2178.

(53) Hino, S.; Lambert, R. M. Chlorine chemisorption and surface chloride formation on iron: adsorption/desorption and photoelectron spectroscopy. *Langmuir* **1986**, *2*, 147–150.

(54) Linsebigler, A. L.; Smentkowski, V. S.; Ellison, M. D.; Yates, J. T. Interaction of chlorine with iron(110) in the temperature range 90-1050 K. *Journal of the American Chemical Society* **1992**, *114*, 465–473.

(55) Dowben, P.; Jones, R. Halogen adsorption on Fe(100): I. The adsorption of Cl2 studied by AES, LEED, work function change and thermal desorption. *Surface Science* **1979**, *84*, 449 – 461.

(56) Lin, R.-J.; Li, F.-Y.; Chen, H.-L. Computational Investigation on Adsorption and Dissociation of the NH_3 Molecule on the Fe(111) Surface. *The Journal of Physical Chemistry C* **2011**, *115*, 521–528.

(57) Grunze, M.; Bozso, F.; Ertl, G.; Weiss, M. Interaction of ammonia with Fe(111) and Fe(100) surfaces. *Applications of Surface Science* **1978**, *1*, 241 – 265.

(58) Momma, K.; Izumi, F. *VESTA3* for three-dimensional visualization of crystal, volumetric and morphology data. *Journal of Applied Crystallography* **2011**, *44*, 1272–1276.

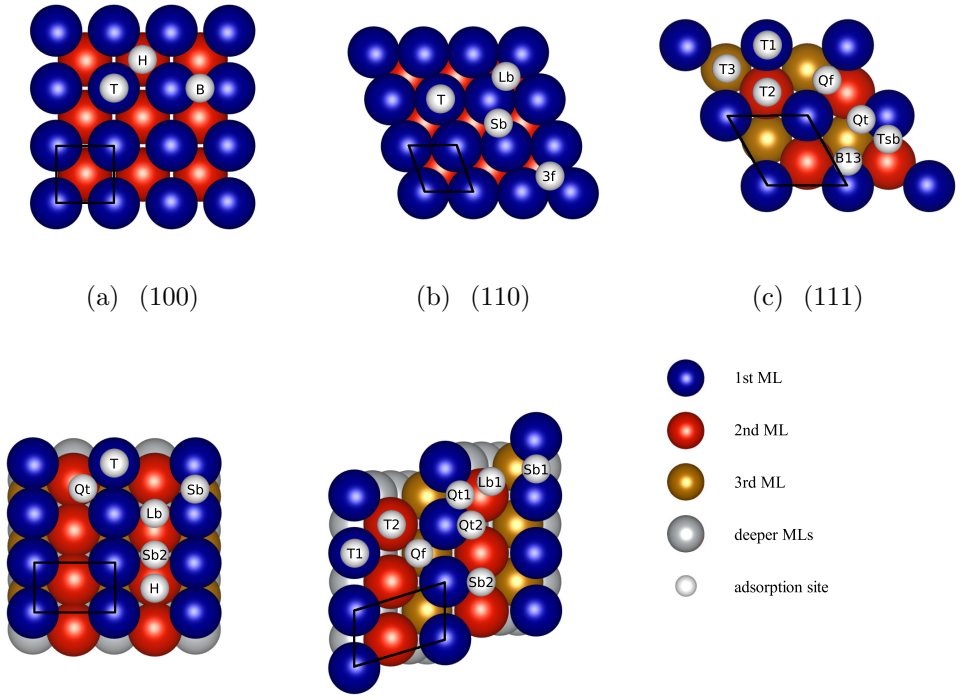

(a) (100) (b) (110) (c) (111)

(d) (211) (e) (310)

Figure 1: Top views of the five investigated surfaces with their 1×1 surface unit cells, indicated by the black quadrangles. The Fe atoms in the first (blue), second (red), third (yellow), and deeper (grey) MLs are shown with the possible high symmetry adsorption sites of each surface (small white). These are: 1(a) B – bridge, H– hollow, T – top; 1(b) 3f – (quasi) 3-fold hollow, Lb – long bridge, Sb – short bridge, T – Top; 1(c) B13 – bridge between Fe in 1st and 3rd layer, Qf – quasi four-fold, Qt – quasi three-fold, T1 (T2, T3) – on top of Fe in the 1st (2nd, 3rd) ML, Tsb – top-shallow bridge; 1(d) H– hollow, Lb – long bridge (between 1st ML Fe atoms), Qt – quasi 3-fold hollow, Sb – short bridge, Sb2 – short bridge between 2nd ML, T – top; 1(e) Lb1 – long bridge between 1st ML Fe, Qf – quasi four-fold, Qt1 (Qt2) – quasi three-fold with two Fe atoms of 1st (2nd) ML, Sb1 (Sb2) – short bridge between 1st (2nd) ML Fe, T1 (T2) – top of 1st (2nd) ML Fe.

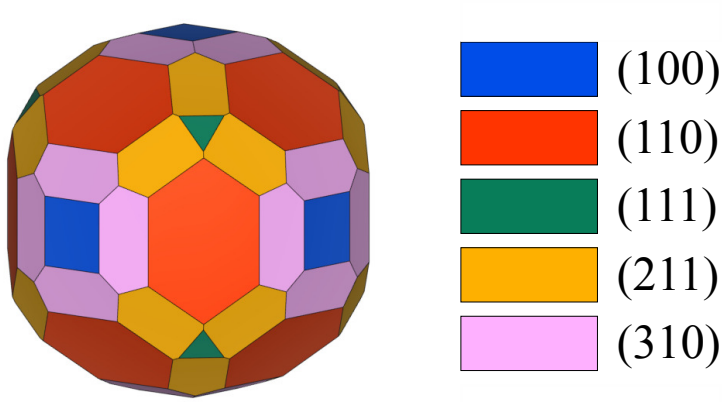

Figure 2: Wulff shape of a bare FeNP according to the γ_{hkl} of Table 1.

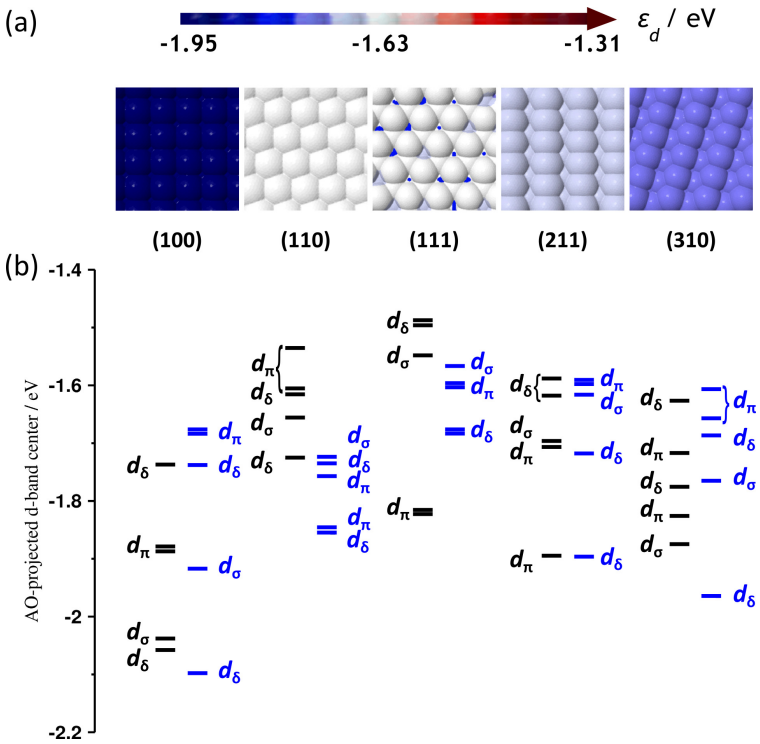

Figure 3: (a) d-band center coordination map including legend with the correspondence between colours and energy scale (in eV); (b) effective d AOs diagram calculated for various Fe(hkl) slabs. Left (in black): surface atoms, right (in blue): lower layer.

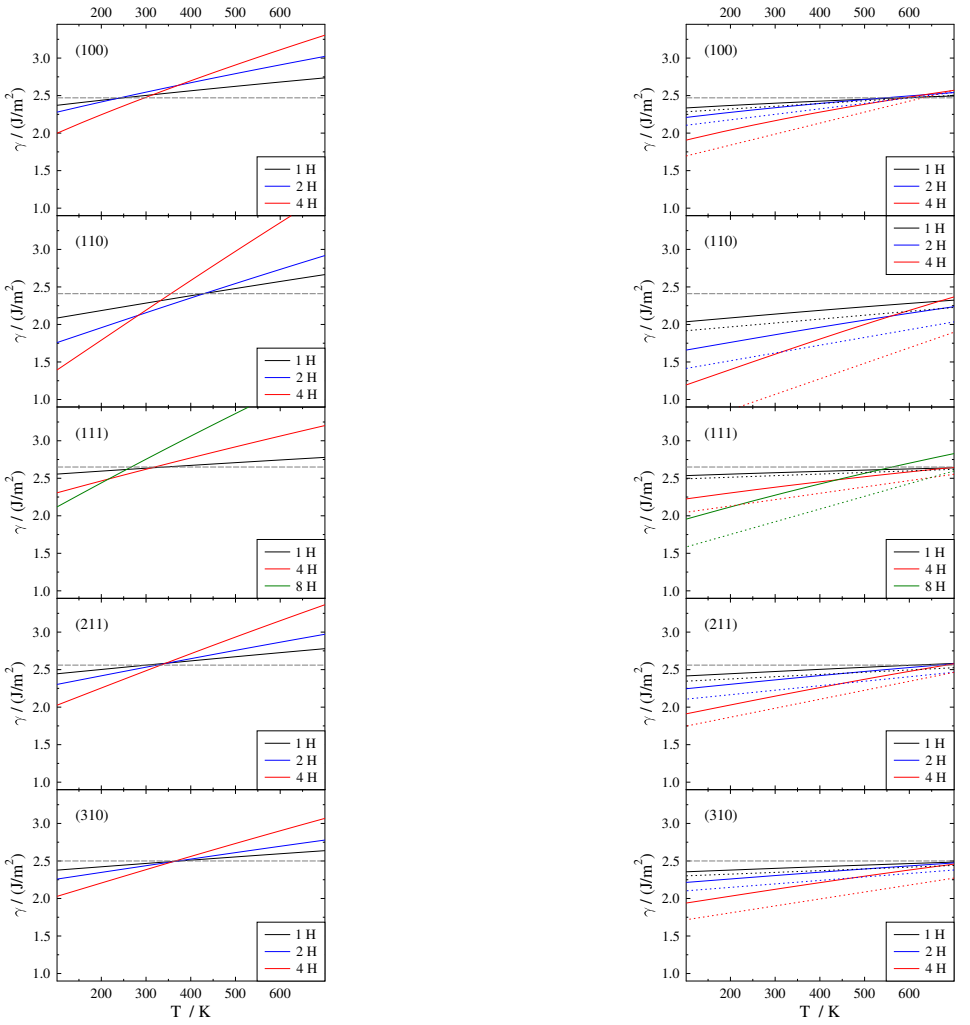

(a) $a/a^\circ = 10^{-7}$ (b) $a/a^\circ = 1$

(c) $T = 150\,\mathrm{K}$ (d) $T = 450\,\mathrm{K}$ (e) $T = 150\,\mathrm{K}$ (f) $T = 450\,\mathrm{K}$

Figure 4: Surface energies of the Fe surfaces at (a) low ($a/a^\circ = 10^{-7}$) and (b) standard ($a/a^\circ = 1$) H_2 activity. Below each graph are the corresponding FeNP Wulff constructions at $T = 150\,\mathrm{K}$ and at $T = 450\,\mathrm{K}$ close to experimental conditions. The dotted lines in (b) represent the surface energies without vibrational terms.

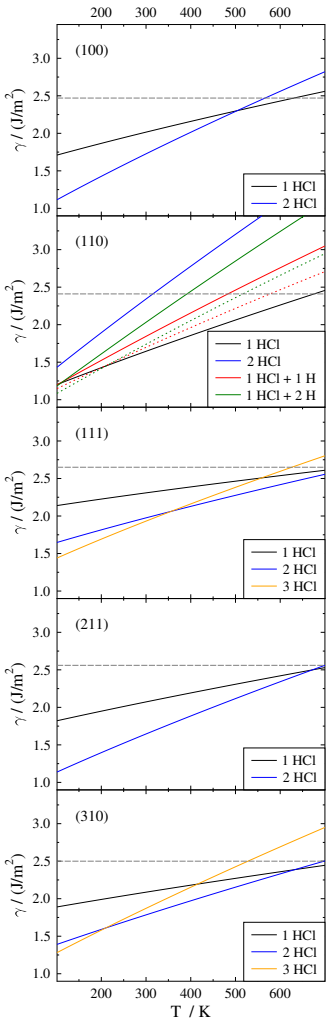

(a) $a/a^\circ = 10^{-7}$

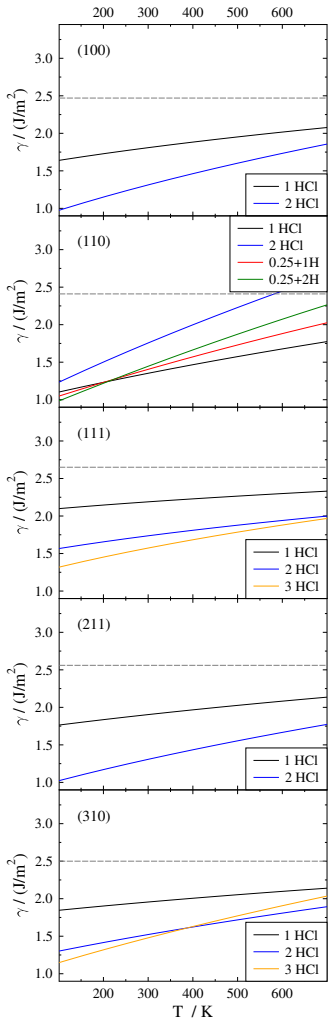

(b) $a/a^\circ = 1$

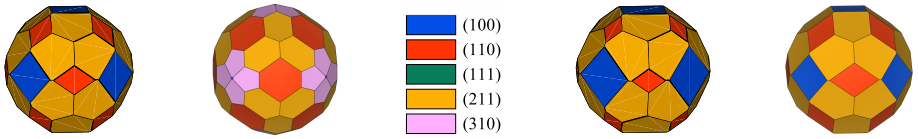

(c) $T = 150\,\mathrm{K}$ (d) $T = 450\,\mathrm{K}$ (e) $T = 150\,\mathrm{K}$ (f) $T = 450\,\mathrm{K}$

Figure 5: Surface energies of the Fe surfaces at (a) low ($a/a^\circ = 10^{-7}$) and (b) standard ($a/a^\circ = 1$) HCl activity. Below each graph are the corresponding Wulff constructions of FeNP at $T = 150\,\mathrm{K}$, rand at $T = 450\,\mathrm{K}$.

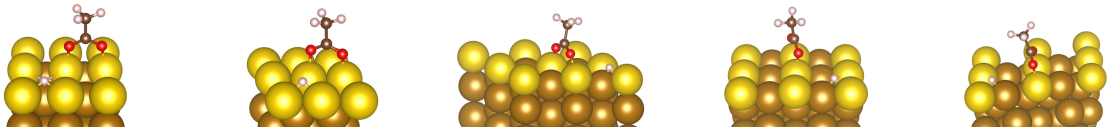

(a) (100) (b) (110) (c) (111) (d) (211) (e) (310)

Figure 6: Adsorption geometries of CH_3COOH at the five different Fe surfaces after dissociation. The Fe top layer is represented by yellow balls, other Fe atoms by light brown ones. Small white (brown, red) balls represent H (C, O, respectively).

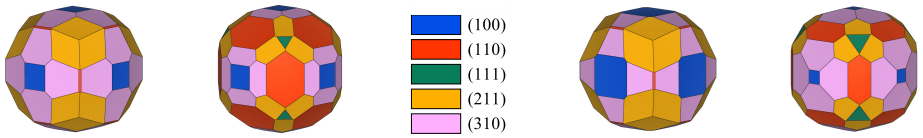

(a) $T = 150$ K (b) $T = 450$ K (c) $T = 150$ K (d) $T = 450$ K

Figure 7: Wulff constructions of Fe NPs under CH_3COOH adsorption at different chemical conditions: (a) and (b) at $a/a^\circ = 10^{-7}$; (c) and (d) at $a/a^\circ = 1$.

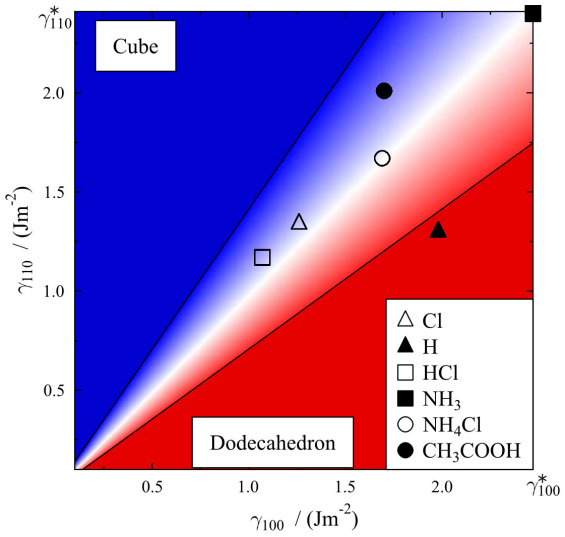

Figure 8: Phase diagram of the tendency of a ligand covered FeNP towards cubic (blue) or dodecahedral (red) shape depending on the γ_{hkl} of the (100) and the (110) facets. Other surfaces are disregarded. The two black solid lines mark the transition towards perfect cubes and dodecahedrons, respectively. Shown are the $\gamma_{100/110}$ pairs of each ligand with the $\gamma_{110}/\gamma_{100}$ ratio closest to $\sqrt{2}$, representing the upper transition line.

For table of contents only